Published by IOP Publishing for Sissa Medialab

Received: *September 30, 2016*
Accepted: *December 15, 2016*
Published: *January 2, 2017*

18th International Workshop on Radiation Imaging Detectors
3–7 July 2016,
Barcelona, Spain

10 μm-thick four-quadrant transmissive silicon photodiodes for beam position monitor application: electrical characterization and gamma irradiation effects

J.M. Rafí,[a,1] **G. Pellegrini,**[a] **D. Quirion,**[a] **S. Hidalgo,**[a] **P. Godignon,**[a] **O. Matilla,**[b] **J. Juanhuix,**[b] **A. Fontserè,**[b] **B. Molas,**[b] **D. Pothin**[c] **and P. Fajardo**[c]

[a] *Instituto de Microelectrónica de Barcelona, IMB-CNM (CSIC), Carrer dels Til·lers s/n, Campus UAB, 08193 Bellaterra, Spain*
[b] *ALBA Synchrotron, Carrer de la Llum 2-26, 08290 Cerdanyola del Vallès, Spain*
[c] *ESRF The European Synchrotron, 71 Avenue des Martyrs, 38000 Grenoble, France*

E-mail: jm.rafi@csic.es

Abstract: Silicon photodiodes are very useful devices as X-ray beam monitors in synchrotron radiation beamlines. Owing to Si absorption, devices thinner than 10 μm are needed to achieve transmission over 90% for energies above 10 keV. In this work, new segmented four-quadrant diodes for beam alignment purposes are fabricated on both ultrathin (10 μm-thick) and bulk silicon substrates. Four-quadrant diodes implementing different design parameters as well as auxiliary test structures (single diodes and MOS capacitors) are studied. An extensive electrical characterization, including current-voltage (I-V) and capacitance-voltage (C-V) techniques, is carried out on non-irradiated and gamma-irradiated devices up to 100 Mrad doses. Special attention is devoted to the study of radiation-induced charge build-up in diode interquadrant isolation dielectric, as well as its impact on device interquadrant resistance. Finally, the devices have been characterized with an 8 keV laboratory X-ray source at 10^8 ph/s and in BL13-XALOC ALBA Synchroton beamline with 10^{11} ph/s and energies from 6 to 16 keV. Sensitivity, spatial resolution and uniformity of the devices have been evaluated.

Keywords: Beam-line instrumentation (beam position and profile monitors; beam-intensity monitors; bunch length monitors); Radiation damage to detector materials (solid state); Si microstrip and pad detectors; X-ray detectors

[1] Corresponding author.

doi:10.1088/1748-0221/12/01/C01004

2017 JINST 12 C01004

Contents

2017 JINST 12 C01004

1 Introduction

Silicon photodiodes are very useful devices as X-ray beam monitors in synchrotron radiation beamlines [1]. In order to be used in transmissive mode and given the absorption properties of silicon, the devices must be thinner than 10 μm to achieve X-ray transmission higher than 90% for photon energies above 10 keV. In a previous study [2], ALBA and IMB-CNM-CSIC reported first results of 10×10 mm^2 single photodiode prototypes fabricated on thin (10 μm) silicon layers for beam intensity monitoring purposes. This work presents four-quadrant photodiodes designed primarily to be used as beam position monitors of synchroton beams, although this type of segmented devices is also of potential interest for astronomy and space applications such as solar tracking systems [3]. Radiation hardness of the involved technologies is a major concern for high-energy physics and space applications.

The devices have been produced on both ultrathin and bulk silicon substrates with different design parameters along with auxiliary technology test structures (single diodes and MOS capacitors). An extensive electrical characterization has been carried out on non-irradiated and gamma-irradiated devices up to doses of 100 Mrad by using both current-voltage (I-V) and capacitance-voltage (C-V) techniques. Special attention has been put into the study of charge build-up in diode interquadrant isolation, as well as its impact on interquadrant resistance. The devices have been characterized with an 8 keV laboratory X-ray source at 10^8 ph/s and in BL13-XALOC ALBA Synchroton beamline with 10^{11} ph/s and energies from 6 to 16 keV. Sensitivity, spatial resolution and uniformity of the devices have been evaluated.

2 Fabrication of 10 μm-thick four-quadrant diodes

The fabrication process is based on a technology developed at Max Planck Institute to fabricate large area thin detectors [4]. The ultra-thin silicon devices are obtained by a combination of direct wafer bonding, wafer thinning, p-on-n device processing and backside deep anisotropic etching processes [2, 4]. The technology is useful for the production of any kind of thin sensors with active back side (pad detectors, strip detectors, etc. . .). Figure 1 shows squematic cross sections illustrating the fabrication process of a four-quadrant diode with its peripheral guard ring. The thicker support frame outside the thin sensitive area allows for safe handling and mounting of the devices.

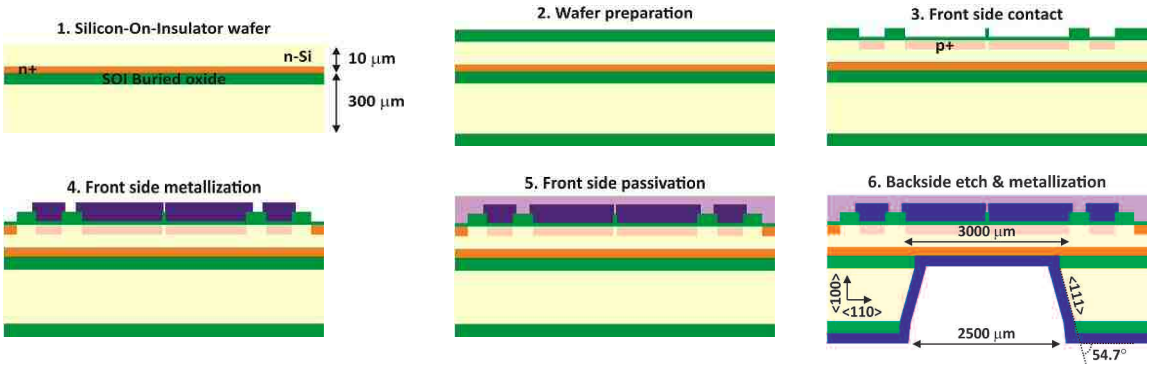

Figure 1. Schematic cross sections (not drawn to scale) illustrating the fabrication process for a four-quadrant diode with its peripheral guard ring.

Figure 2 shows front and back side pictures of a 100 mm diameter wafer with the final devices fabricated at IMB-CNM. From the backside picture (figure 2(b)), the thin active areas of the devices, generated by means of backside deep anisotropic etching, can be clearly appreciated. The mask design basically includes single diodes (not segmented in four quadrants) and four-quadrant diode variants implementing different space gap between quadrants as well as various geometries for the front side metal layer. A fixed size die (4400 μm $\times$ 4400 μm) is used for all devices. Furthermore, metal-oxide-semiconductor (MOS) capacitors using as gate dielectric the interquadrant isolation oxide used for the four-quadrant diode structures are also available.

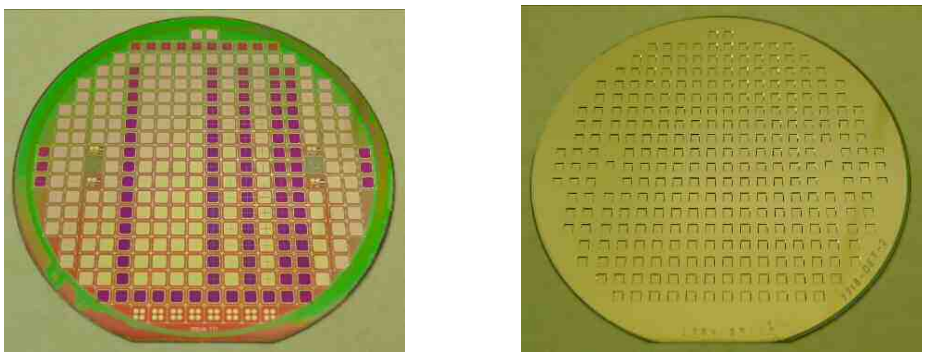

(a) **(b)**

Figure 2. (a) Front and (b) back side pictures of a processed Si wafer showing the final devices.

2017 JINST 12 C01004

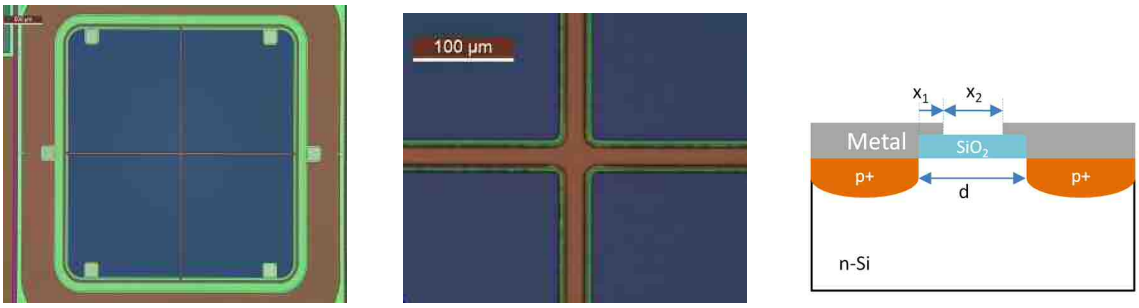

(a) (b) (c)

Figure 3. (a) Picture of a 10 μm-thick four-quadrant diode fabricated at IMB-CNM, (b) detail of the centre of the diode and (c) sketch showing the definition of the interquadrant distance "d", as well as the metal overlapped and non-overlapped field regions (x_1 and x_2, respectively).

Figure 3 shows pictures of one of the final 10 μm-thick four-quadrant diodes, together with a sketch presenting the definition of the interquadrant distance (d), as well as the metal overlapped and non-overlapped field regions (x_1 and x_2, respectively). Isolation oxide, represented as "SiO_2" in figure 3(b), it is indeed a dielectric stack composed by a thermally grown SiO_2 layer of about 520 nm plus a deposited 180 nm Si_3N_4 layer, which was used as a mask for the wafer backside thinning process.

3 Electrical characterization and gamma irradiation effects

The processed wafers were diced into single chip devices and some single diodes, four-quadrant diodes and MOS capacitors were subjected to unbiased gamma irradiations (the terminals of the devices were left floating) at room temperature. The irradiations were carried out at Sandia National Laboratory (U.S.A.) for three different doses (10 Mrad, 30 Mrad and 100 Mrad). Current-voltage (I-V) and Capacitance-Voltage (C-V) characteristics were measured both, on wafer and after wafer dicing into single chips. The measurements were done in a light-proof and electrically shielded probe station by using an HP 4155B semiconductor parameter analyzer and an Agilent 4284A Precision LCR Meter.

3.1 Diode current-voltage characteristics

The I-V characteristics of the diodes were measured with three independent HP 4155B source monitor units (SMUs) connected to the diode, ring and backside terminals. While zero potential was applied to the diode and ring terminals, a voltage sweep was performed on the backside terminal. Figure 4 shows the diode current density measured for three different 10 μm-thick single diodes (not segmented in four quadrants) before and after gamma irradiation at three different doses (10 Mrad, 30 Mrad and 100 Mrad). From the figure, a progressive increase of leakage current in reverse bias operation is observed for increasing gamma irradiation dose. The current at 2 V reverse voltage is found to increase by factors of about 2.2, 3.2 and 7 for diodes irradiated at 10 Mrad, 30 Mrad and 100 Mrad, respectively. In what concerns the reverse bias breakdown voltage, it is mantained above 40 V and no clear radiation-induced effect was observed.

2017 JINST 12 C01004

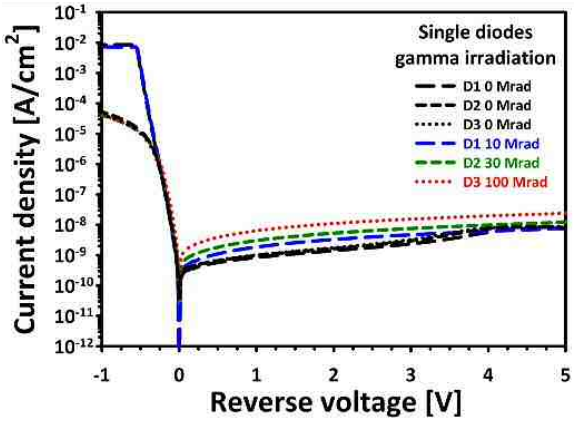

Figure 4. Diode current density measured for three different 10 μm-thick single diodes before and after gamma irradiation at three different doses (10 Mrad, 30 Mrad and 100 Mrad).

It has to be mentioned that the diced chips presented similar I-V characteristics before irradiation than previous measurements performed on-wafer. No significant changes were observed for reverse current levels, only slightly lower direct conduction current levels were measured in the diced devices, what could be attributed to a higher contact resistance for those samples. No significant radiation-induced effect was observed for the measured characteristics in direct operation.

The diode reverse current characteristics of the non-irradiated devices present a slight change of slope for voltages around 3 or 4 V that is attributed to reaching full depletion condition of the thin silicon layer. However, this effect is not observed in the irradiated diodes, as it becomes hidden by radiation-induced increase of the reverse current.

3.2 Isolation oxide charges

In order to evaluate any possible impact of radiation-induced charge build-up in diode interquadrant isolation dielectric of the segmented four-quadrant diodes, several metal-oxide-semiconductor (MOS) capacitors that use the same isolation oxide as gate dielectric were also studied. Figure 5(a) shows the C-V characteristics measured at 10 kHz for three different MOS capacitors before and after irradiation. From the capacitance values in accumulation condition, a mean value of 620 nm, with a standard deviation of 10 nm, was obtained for the electrical oxide thickness. These results are in excellent agreement with the values measured by interferometry for the SiO_2 field oxide (in the range of 517–527 nm) plus the deposited Si_3N_4 thickness (185–189 nm). Indeed, an equivalent SiO_2 oxide thickness (EOT) of 613–625 nm was obtained from the interferometry measurements, assuming a relative permittivity of 7.5 for the Si_3N_4 layer.

From figure 5(a), a clear strecht-out and radiation-induced shift of C-V curves towards negative gate voltages is observed. In this way, flat band voltage (V_{fb}) shifts of around −28 V, −43 V and −60 V were obtained for the devices irradiated at 10 Mrad, 30 Mrad and 100 Mrad, respectively. This is indicative of a radiation-induced positive charge build-up. An estimation of the effective trapped charge density (N_{eff}), defined as a fixed charge located at the silicon/dielectric interface, has been obtained from the comparison of the extracted V_{fb} values with the figures expected for an ideal MOS structure with 4.25 eV metal work function, corresponding to the aluminium gate

2017 JINST 12 C01004

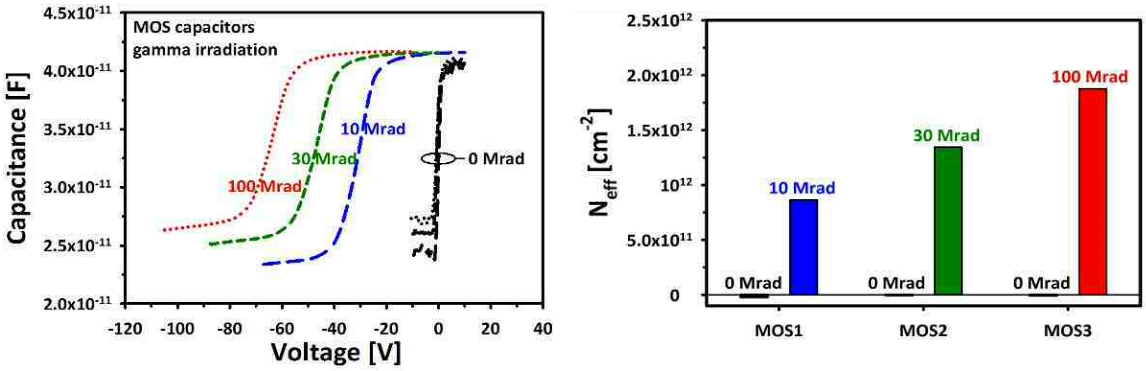

(a) (b)

Figure 5. (a) C-V characteristics measured at 10 kHz from inversion to accumulation for three different MOS capacitors (using the diode interquadrant SiO_2 field oxide) before and after gamma irradiation at three different doses. MOS capacitor area is $8.17 \times 10^{-3}\,cm^2$. (b) Corresponding extracted values for effective trapped charge densities (N_{eff}) in the dielectric.

electrode [5]. From figure 5(b), slightly negative N_{eff} values, in the range of $-1.8 \times 10^{10}\,cm^{-2}$ to $-1.8 \times 10^{9}\,cm^{-2}$, have been obtained for non-irradiated devices (assuming a theoretical V_{fb} value of -0.16 V for a MOS capacitor on n-type silicon). However, positive N_{eff} values in the range of $8.7 \times 10^{11}\,cm^{-2}$, $1.3 \times 10^{12}\,cm^{-2}$ and $1.9 \times 10^{12}\,cm^{-2}$ are obtained for the devices irradiated at 10 Mrad, 30 Mrad and 100 Mrad, respectively.

With the aim to investigate the presence of any possible radiation-induced hysteresis on the C-V curves, some characteristics were also measured at 10 kHz for accumulation to inversion voltage sweep direction. Hysteresis was quantified as the difference between the extracted V_{fb} values corresponding to the two voltage sweep directions. While no significant hysteresis was found for the non-irradiated MOS capacitors, slight clockwise hysteresis is found to appear and progressively increases with irradiation dose. In this way, values around 1.3 V, 2.3 V and 4.2 V were obtained for the devices irradiated at 10 Mrad, 30 Mrad and 100 Mrad, respectively. The observed hysteresis on n-type Si capacitors is attributed to silicon/dielectric interface and near interface border traps [6], which may get charged and exchange electrons with the silicon substrate depending on the voltage sweep direction [5, 7].

In view of the significant radiation-induced V_{fb} shift of the C-V curves, as well as the observed hysteresis, C-V characteristics were also measured at different frequencies. Figure 6(a) shows the results obtained for non-irradiated and 100 Mrad gamma-irradiated MOS capacitors. Extracted values for effective trapped charge densities in the dielectric (N_{eff}) are also given in figure 6(b). From the figures, no frequency dependence is observed for devices before irradiation, however, a clear frequency dependence is observed after irradiation. This evidences the existence of a spectrum of radiation-induced defects which can follow different frequencies. As expected, the observed radiation-induced V_{fb} shift is higher for low frequency measurements, where most of the defects can be filled. On the other hand, less radiation-induced V_{fb} shift is observed for the highest frequencies, where a significant amount of defects can't follow the measurement frequency and do not contribute to the C-V signal [7].

2017 JINST 12 C01004

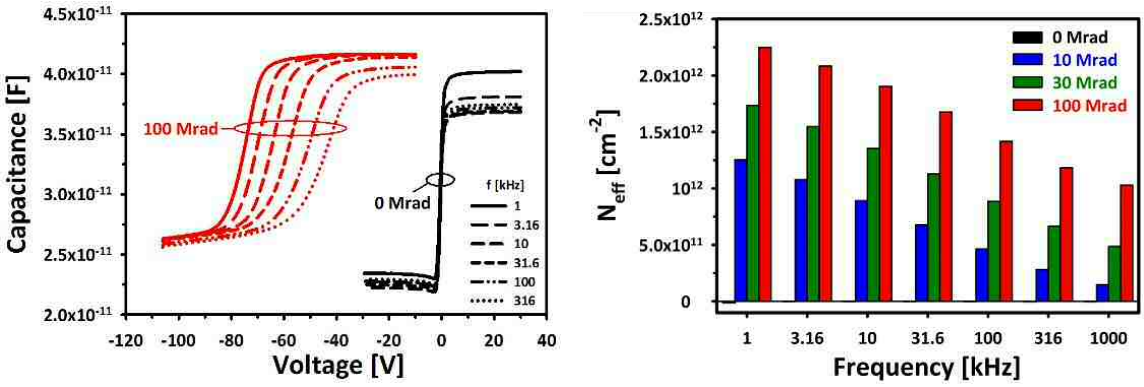

Figure 6. (a) C-V characteristics measured at different frequencies from inversion to accumulation for non-irradiated and 100 Mrad gamma-irradiated MOS capacitors, with area 8.17×10^{-3} cm^2. (b) Extracted values for effective trapped charge densities (N_{eff}) in the dielectric for non-irradiated and gamma irradiated MOS capacitors measured at different frequencies.

From figure 6(b), significant differences in N_{eff} are obtained as a function of frequency for the different irradiated samples. In this way, for example, for the case of MOS devices irradiated at 100 Mrad, N_{eff} values ranging from 2.25×10^{12} cm^{-2} to 1×10^{12} cm^{-2} are extracted for C-V measurement frequencies between 1 kHz and 1000 kHz. The magnitude of the observed radiation-induced positive charge build-up is in agreement with results obtained for comparable dielectric layers and radiation doses in previous experiments with more conventional radiation detectors technologies [8–10]. Furthermore, similar frequency dependences for C-V degradation have been also observed [10, 11]. In particular, an empirical relationship for the V_{fb} dependency on frequency (f) has been drawn ($V_{fb} = a \cdot \ln(f) + b$), with a and b the slope and intercept fitting parameters. From the fitting of 10 Mrad, 30 Mrad and 100 Mrad results in figure 6(b), the obtained a slope values are in the range of 12 to 13 Volts per decade of frequency. These values are about 5.5 times higher than the ones reported by J. Wüstenfeld [10] for 160 nm SiO_2 layers irradiated at a dose of 50 Mrad. However, when taking into account the factor close to 4 between the electrical oxide thicknesses, the slope values become in reasonable agreement.

3.3 Interquadrant resistance characteristics

In order to investigate possible radiation-induced effects on the interquadrant resistance of the segmented diodes, two sets of devices with different geometry parameters (module A with d=10 μm, $x_1 = 3$ μm, $x_2 = 4$ μm and module B with d=6 μm, $x_1 = 1$ μm, $x_2 = 4$ μm) were also subjected to the gamma irradiations. The devices were measured before and after irradiation. Four independent HP 4155B source monitor units (SMUs) were connected to the first quadrant, to the second, third and fourth quadrants shorted together, to the guard ring and to the backside terminal. Current versus voltage curves were measured by applying a limited V_2 voltage sweep (from −1 V to +1 V) to the three connected neighbour quadrants while measuring the I_1 current in the other quadrant that was kept at zero potential as well as the guard ring. These curves were measured for several diode backside reverse voltages. An estimation of interquadrant resistance was obtained from the slope of

2017 JINST 12 C01004

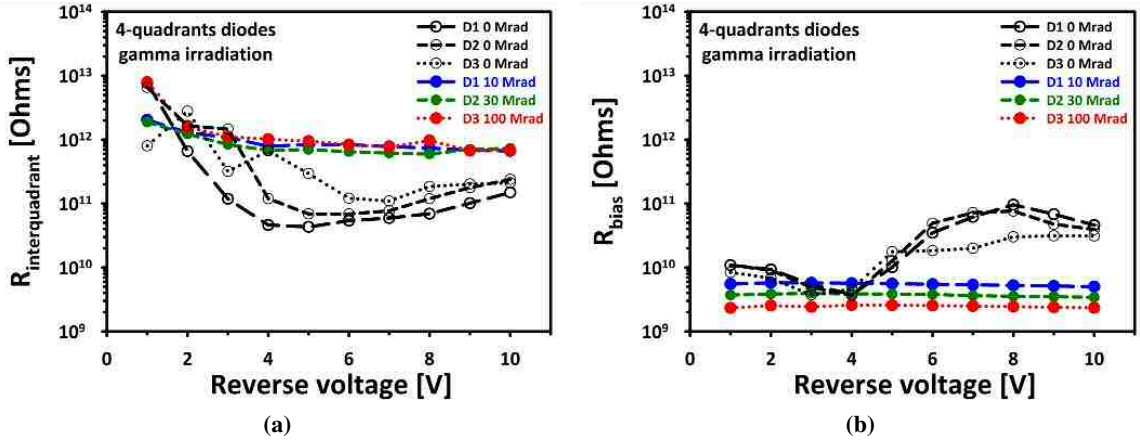

Figure 7. (a) Interquadrant resistance and (b) bias resistance as a function of substrate reverse voltage extracted before and after gamma irradiation for three four-quadrant diodes.

I_1 versus V_2 characteristics ($R_{interquadrant} = 1/|(dI_1/dV_2)|$). Similarly, an estimation of bias resistance was obtained from the slope of I_2 versus V_2 characteristics ($R_{bias} = 1/|(dI_2/dV_2)|$). The slopes were obtained by means of linear curve fits of the measured characteristics at the various diode backside reverse biases. High $R_{interquadrant}$ and R_{bias} values (in the range of 10^{11} Ω and 10^{10} Ω, respectively) were obtained for the non-irradiated four-quadrant segmented diodes belonging to either module A or module B geometries.

In accordance with the previous results from I-V measurements on single diodes, higher reverse bias leakage currents were obtained when increasing irradiation dose for all the segmented diodes of modules A and B. However, in most cases gamma-irradiation was found to sligthly improve the $R_{interquadrant}$ values. This can be appreciated for example in the results of figure 7(a) for module A devices before and after gamma irradiation. The higher $R_{interquadrant}$ values for gamma-irradiated devices could be explained by the presence of radiation-induced positive charges in the isolation dielectric (as derived from the C-V measurements on MOS capacitors), which would lead the n-type silicon surface to a deeper accumulation condition, thus improving interquadrants isolation. On the other hand, as it could be envisaged, R_{bias}, which is merely depending on diode leakage current, is slightly degraded with irradiation dose (figure 7(b)), being this in agreement with the radiation-induced leakage current increase observed for the single diodes results.

4 Preliminary X-ray characterization

The functional response of the four-quadrant devices as X-ray beam position monitors has been assessed. First results about characterization of the devices with an 8 keV Cu anode microfocus laboratory X-ray source have shown good spatial uniformity for the photocurrent response of the four-quadrant diodes (figure 8(a)). Furthermore, good sensitivity and spatial resolution have been also obtained during first tests at the ALBA synchrotron BL13-XALOC beamline [12]. A sensitivity (responsivity) value of 12.7 mA/W, matching with a theoretical 7 μm silicon depletion layer, has been obtained with a 10 keV X-ray beam of 10^{11} ph/s. From the distance between the centers of the

2017 JINST 12 C01004

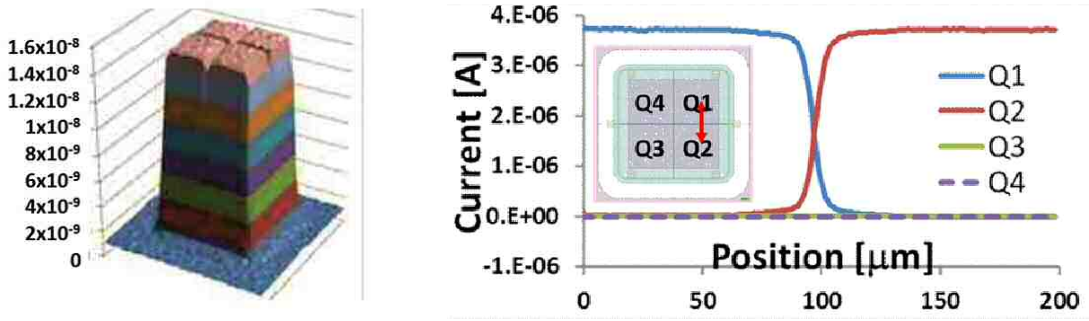

(a) (b)

Figure 8. (a) Spatial uniformity map for the total diode photocurrent response to a 100 μm FWHM 8 keV X-ray beam with 10^8 ph/s. (b) Measured current at the different quadrants during a Q1 to Q2 quadrant transition (inset) of a 12.3 μm FWHM 10 keV X-ray synchrotron beam.

two Gaussians corresponding to the derivative of the measured current at two adjacent quandrants (figure 8(b)), effective functional gaps of 1.4 μm and 1.2 μm in the horizontal and vertical scan directions have been respectively obtained for a module B device. As it should be, it is remarkable the fact of obtaining quite similar values in both axes, meanwhile the beam size was five times bigger in the horizontal direction [12].

5 Summary

Segmented four-quadrants diodes, intended for X-ray beam alignment purposes, have been fabricated on ultrathin silicon layers. Electrical characterization has been carried out on non-irradiated and gamma-irradiated single diodes, MOS capacitors and four-quadrant diodes up to 100 Mrad doses. Special attention has been devoted to the study of radiation-induced charge build-up in diode interquadrant isolation dielectric, as well as its impact on device interquadrant resistance. First results from X-ray characterization in BL13-XALOC ALBA Synchroton beamline show good sensitivity, spatial resolution and uniformity for the fabricated devices.

Acknowledgments

This work has been partially financed by Spanish Ministry of Education and Science through the Particle Physics National Program FPA2015-69260-C3-3-R and the European Project Advanced European Infrastructures for Detectors and Accelerators (AIDA-2020-INFRAIA-2015). The authors thank V. Fadeyev from SCIPP and S. Seidel and M. Hoeferkamp from Univ. of New Mexico for their help with the irradiations, as well as staff at the Gamma Irradiation Facility of Sandia National Laboratory, especially Dr. M. Wasiolek and Dr. D. Hanson.

2017 JINST 12 C01004

References

[1] M.R. Fuchs et al., *Transmissive x-ray beam position monitors with submicron position- and submillisecond time resolution*, *Rev. Sci. Instrum.* **79** (2008) 063103.

[2] C. Cruz et al., *10 μm thin transmissive photodiode produced by ALBA Synchrotron and IMB-CNM-CSIC*, 2015 *JINST* **10** C03005.

[3] P. Roth, A. Georgiev and H. Boudinov, *Design and construction of a system for sun-tracking*, *Renew. Energ.* **29** (2004) 393.

[4] L. Andricek et al., *Processing of ultra-thin silicon sensors for future e^+e^- linear collider experiments*, *IEEE Trans. Nucl. Sci.* **51** (2004) 1655.

[5] J.M. Rafí et al., *2 MeV electron irradiation effects on the electrical characteristics of metal-oxide-silicon capacitors with atomic layer deposited Al_2O_3, HfO_2 and nanolaminated dielectrics*, *Solid State Electron.* **79** (2013) 65.

[6] D.M. Fleetwood, *"Border traps" in MOS devices*, *IEEE Trans. Nucl. Sci.* **39** (1992) 269.

[7] D.K. Schroder, *Semiconductor material and device characterization*, John Wiley & Sons, New York (1990).

[8] J. Zhang et al., *X-ray induced radiation damage in segmented p + n silicon sensors*, Jeju, Korea, 16–21 September 2012, PoS(Vertex 2012)019.

[9] J. Schwandt et al., *Study of high-dose X-ray radiation damage of silicon sensors*, *Proc. SPIE* **8777** (2013) 87770K.

[10] J. Wüstenfeld, *Characterisation of ionisation-induced surface effects for the optimisation of silicon-detectors for particle physics applications*, Ph.D. Thesis, University of Dormund (2001).

[11] J. Schwandt, *Design of a radiation hard silicon pixel sensor for X-ray science*, Ph.D. Thesis, University of Hamburg (2014).

[12] J. Juanhuix et al., *Developments in optics and performance at BL13-XALOC, the macromolecular crystallography beamline at the Alba Synchrotron*, *J. Synchrotron Rad.* **21** (2014) 679.

2017 JINST 12 C01004